



Enhancing PKM accuracy by separating actuation and measurement. A 3-*dof* case study.

David Corbel, Olivier Company, Sébastien Krut and François Pierrot*
LIRMM, Univ. Montpellier 2, CNRS
161, rue Ada, 34392 Montpellier, France

Abstract

This paper propose an approach for enhancing PKM accuracy by separating actuation and measurement. The interest of Separation Actuation & Measurement concept (SAM) is exposed and a definition of sensor redundancy used for designing the measurement device is given. Then, the design of a parallel Machine-Tool (MT) prototype with a independent measuring system, MoM3, is presented as well as the optimization of its measuring system. Finally, the control schemes used on the prototype are presented and the experimental results show the efficiency of SAM applied to a MT.

1 Introduction

Designing a fast, accurate and stiff Machine-tool (MT) is really a hard task. To take up this challenge, MT designers took their inspiration from recent advances in robot kinematic architectures, in particular Parallel Kinematics Machines (PKMs) [1]. PKMs are already used with success in some industrial domains¹.

Nowadays, two well known types of PKMs are transferred to the MT industry:

*Corresponding author: pierrot@lirmm.fr

¹<http://www.parallemic.org/WhosWho/CompPKM.html>

- The hexapods, where six variable length struts link a traveling plate to a base. The first PKM belonging to this family was proposed by Gough [2].
- The Delta robot, invented by Prof Clavel [3], which is a lower mobility PKM (displacements of the traveling plate are restricted to three translations).

The Variax was the first MT inspired by the hexapod architecture [4], and until today, a lot of industrial machines based on this architecture are built: Octahedral Hexapod by Ingersoll, the P1000/P2000/P3000 Hexapods by PRSCO, or the HexaM by Toyoda (even though HexaM is not strictly speaking an "hexapod" since it is not made with 6 telescopic legs). Concerning the Delta kinematics, its version with linear actuators is used on MTs as for UraneSX [5] that can reach up to 5g in its workspace or Quickstep by Krause & Mauser [6].

The main interest for using parallel architecture on MTs is to take advantage of their high dynamical capabilities. These architectures can reach high accelerations because of the light weight of their movable elements compared to serial architectures.

However, whatever the architecture is, geometrical calibration is required to get the best accuracy. The calibration tries to identify model parameters that enhance the machine accuracy [7]. Once these parameters are identified, the model runs "open loop", ie the machine behavior is expected to be the one that has been modeled and identified whatever the stresses in machine components are. For Cartesian classical MTs, the identification can be done axis per axis. Parameter identification can be very accurate as the problem is decoupled. Identifying PKM parameters according to this principle is not possible as all axes are coupled in the model. A full calibration of the model must be done, but it always

ends in a compromise between the number of parameters and the numerical stability [8].

Moreover, for MTs based on parallel architecture, geometrical calibration is not sufficient. To benefit from the high dynamics of the parallel architecture, the use of light elements is necessary and therefore the stiffness of the machine can sometimes be low [9]. This low stiffness of parallel mechanisms is a drawback when they are used in MTs. One solution consists to add redundancy in the architecture [10]. Another solution consists in modeling the deformations using an elastic model of the structure [11] [12] [13]. This solution is interesting to compensate the gravity effects or when the efforts on the end-effector are known but it is seldom the case.

The basic problem in machining is to impose accurate end-effector positioning regarding the part to be machined. The best way to deal with accuracy is to always be able to know the end-effector pose (position and orientation) relative to the part accurately, ie with a quality as close as possible to the metrological one. This can be done by measuring directly the end-effector pose. One way to proceed is to use non-contact full pose measurement system, like vision system [14]. According to [15], 3D visual servoing reduces the complexity of parallel robot Cartesian control. But there is still ongoing research on this topic and, even if algorithms are available, they are not able today to guarantee the requested resolution on the whole workspace of the machine. Moreover, the refreshment rate is not high enough for the control loop, but it is still a promising way of research for the future.

However, visual servoing illustrates the idea of having independence between the measurement chain and the actuation chain. The principle of Separation between Actuation and Measurement (SAM) relies on this independence. SAM allows to guarantee the exact measurement of the end-effector pose therefore a very accurate end-effector positioning.

First, the principle of SAM is explained in section 2. To prove the feasibility and the efficiency of this concept an actuated PKM (a Delta robot) combined with a passive measuring PKM (a Gough platform) is presented in section 4. Then, the optimization of the Gough platform is recalled in section 5. Finally, the control laws used on the mechanism are described (section 6) and the experimental results are shown (section 7).

2 Separation between actuation and measurement

2.1 Motivations

On classical serial or parallel MTs, measuring systems are close to actuators (e.g.: encoders attached to the motors) or close to guideways (e.g.: linear scale on a prismatic joint) (Fig. 1a and 2a). In most cases, these measuring systems do not give any information about (i) assembly errors (Fig. 1b and 2b) or (ii) deformations of the structure (Fig. 1c, 2c). Fig. 3 illustrates this problem for the general case: on a classical machine, with serial or parallel kinematics, most components involved in the measurement chain have to sustain loads coming from the process (e.g.: cutting forces) and suffer from the same assembly errors or thermal effects because they belong to the very same force and motion transmission chain.

The concept of SAM comes from these observations. The idea is to create a measuring system as independent as possible from the force transmission system and as sensitive as possible to the assembly errors and deformations of the mechanical structure. Ideally, the measuring system must be linked only to the ground and the end-effector to insure this independence (Fig. 4). This concept is not completely new: it has been described in

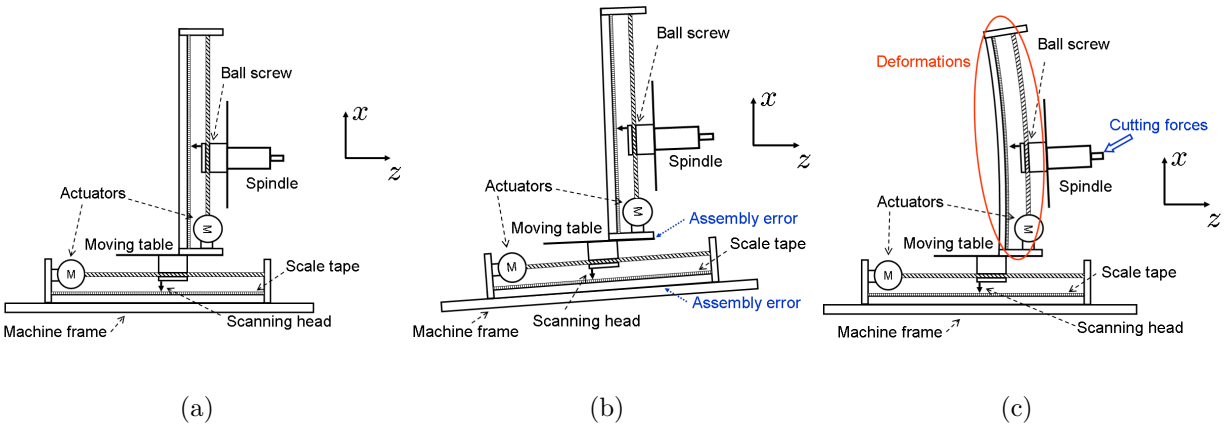


Figure 1: (a) Classical serial MT, (b) with assembly errors, (c) with deformations

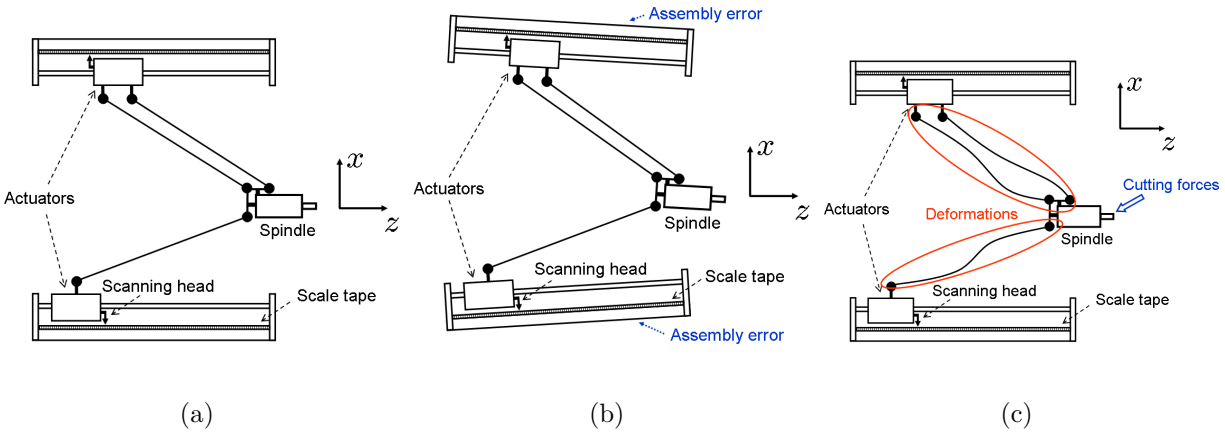


Figure 2: (a) Parallel MT, (b) with assembly errors, (c) with deformations

earlier works. David used this concept for the design of a Coordinate Measuring Machine (CMM) [16]; in seminal work by Hale and Slocum several important principles and techniques to design precision machines were proposed [17] [18], among which the SAM concept for high precision machine-tools; Lahousse [19] resorted to the same principle for designing a measuring device with nanometer resolution.

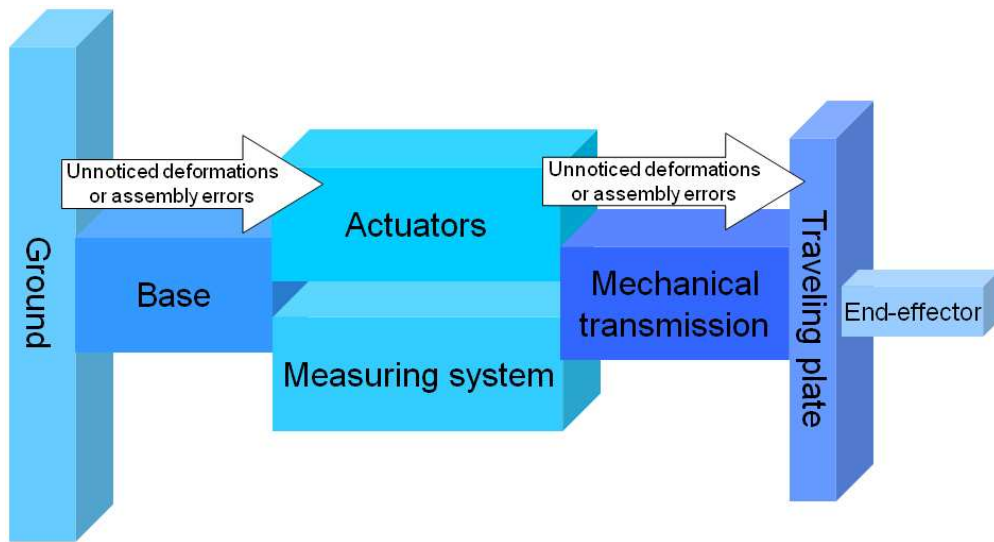


Figure 3: Classical association of actuation and measurement on robots

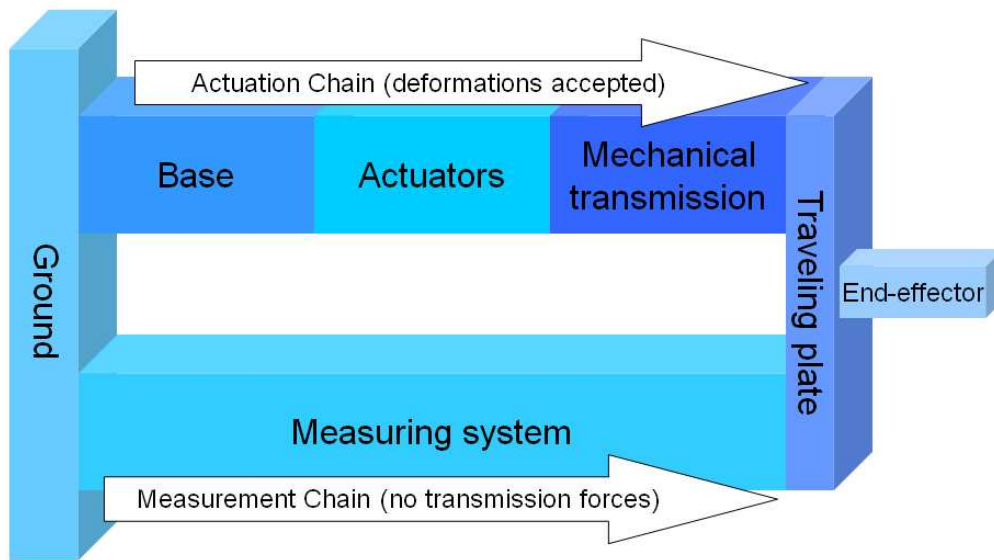


Figure 4: Metrology of robots with SAM

2.2 Actuation chain

Following the concept of SAM, the main function of the actuation chain is to generate and transmit forces to move the end-effector.

As the position and orientation of the traveling plate are measured directly by an independent measuring system, even if some machining or assembly errors exist, they do not influence the accuracy of the machine, as long as a control loop relying on these measures can compensate for the errors.

However, the displacement resolution of the end-effector must be compatible with the defined task and so backlashes and friction effects must be sufficiently low to insure this compatibility.

2.3 Measurement chain

Some features concerning the measurement chain must be taken into account during the design phase:

- (i) The measuring system must measure directly (or almost directly) the end-effector pose.
- (ii) The acquisition frequency must be compatible with real-time control needs (typically: above 1kHz).
- (iii) The positioning capabilities (resolution, repeatability and accuracy) of the measuring system must be compatible with the positioning capabilities required for the task to be achieved.
- (iv) The measuring system must transmit no force.

(v) The measuring system must not interfere with the actuated mechanism.

Measurement systems can be split into two categories:

- without contact; this could be LASER based sensors or cameras for artificial vision;
- with contact; this could be serial measurement arms or systems with parallel kinematics.

A key question regarding the measuring system is: how many pieces of information are necessary to control accurately the machine? Answering this question requires the definition of sensor redundancy.

3 Sensor redundancy

3.1 Definition

Let us define :

- C is the sensor space dimension. It corresponds to the number of independent measures given by the set of sensors.
- M is the dimension of space wherein the end-effector evolves.
- D is the number of the robot degrees of freedom (*dof*).
- O is the spatiality² of the traveling plate.

²Number of independent relative velocities between the base and end-effector of the machine [20]

Definition : *The degree of sensor redundancy ($dosr$) is equal to $C - (M - O + D)$.*

Then, three cases can be distinguished :

- $dosr < 0$, the mechanism is "under-measured";
- $dosr = 0$, the mechanism is "iso-measured";
- $dosr > 0$, the mechanism is "over-measured", and so, there is a sensor redundancy.

One important aspect of this definition is how the variable M is considered. Two cases have to be analyzed: "perfect" case and "imperfect" case. In the "perfect" case, M is equal to the spatiality of the mechanism, O . In the "imperfect case", M is larger than O . Let's take some examples to illustrate the definition.

3.2 Examples

3.2.1 1D example

Fig. 5 shows a solid which moves along a prismatic joint ($D = 1, O = 1$). In the "perfect" case, only 1 measure ($M = 1$) is sufficient to have an "iso-measured" mechanism: $dosr = 1 - (1 - 1 + 1) = 0$. In an "imperfect" case, the solid may evolve not only along x axis but have some parasitical movements along y axis (Fig. 5b). Then, M would be equal to 2 and $dosr$ becomes negative. In such a case, additional measures should be added to recover "iso-measurement".

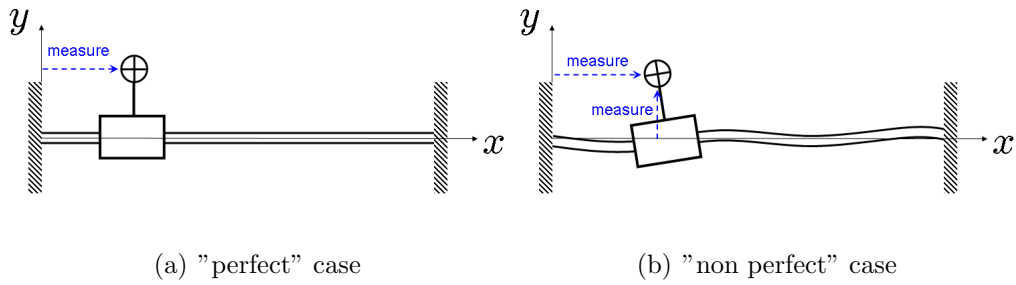


Figure 5: Solid along a prismatic joint

3.2.2 Kinematic redundancy

The definition of the sensor redundancy given in this paper can deal with kinematically redundant mechanisms and mechanisms with actuation redundancy. Let's start with kinematically redundant mechanisms.

First, the definition of kinematic redundancy is recalled: *kinematic redundancy appears when, for a given end-effector velocity and a given pose, there is an infinite number of corresponding joint velocities.*

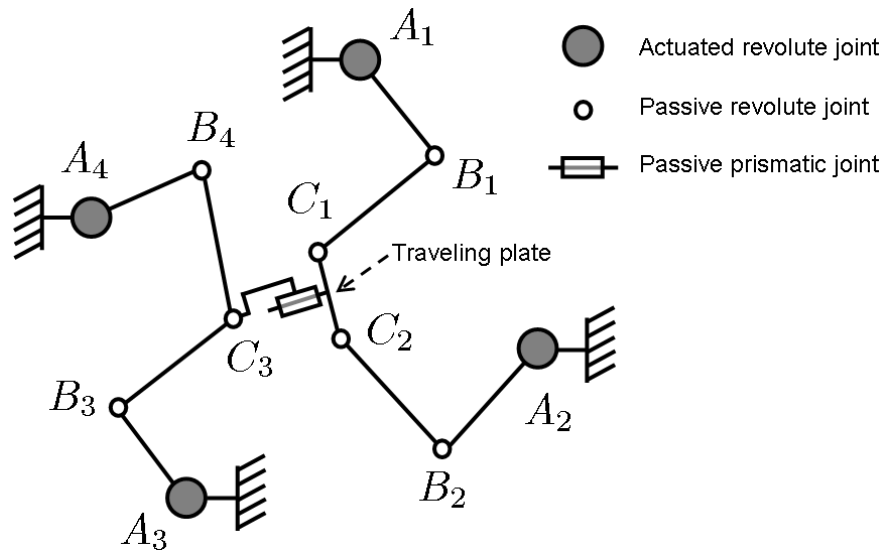


Figure 6: Kinematically redundant parallel manipulator

As an example, Fig. 6 shows a kinematically redundant mechanism with 4 *dof* and a

end-effector spatiality equal to 3 ($D = 4, O = 3$). The "perfect" case is considered here ($M = O$) and only the actuated revolute joint are measured ($C = 4$). For this mechanism, the $dosr$ is equal to 0. So, in the "perfect" case, this kinematically redundant mechanism is "iso-measured", even though it is equipped with more sensors than its spatiality.

3.2.3 Actuation redundancy

The definition of actuation redundancy is the following: *actuation redundancy appears when, for a given force/wrench acting on the end-effector and a given pose, there is an infinite number of corresponding joint forces/torques.*

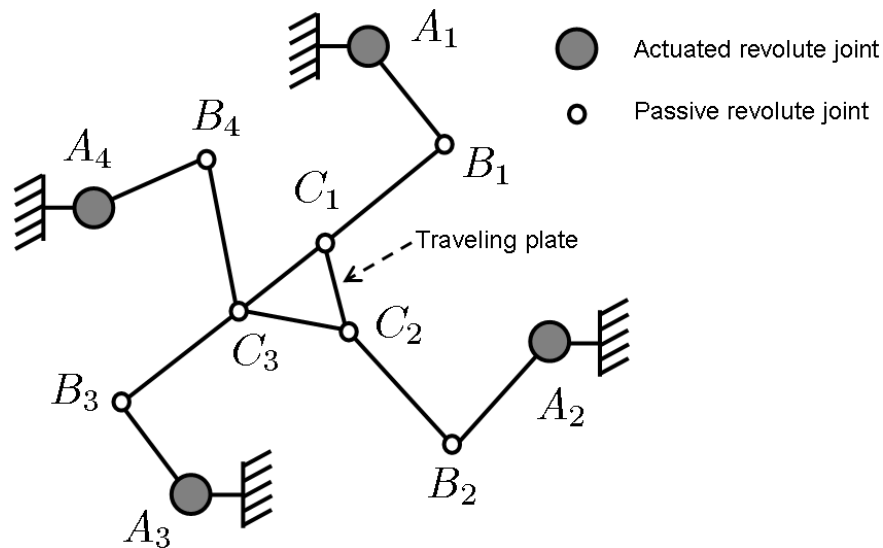


Figure 7: Parallel manipulator with actuation redundancy

As an example, Fig. 7 shows a mechanism with actuation redundancy with 3 dof and a end-effector spatiality equal to 3 ($D = 3, O = 3$). The "perfect" case is considered here ($M = O$) and only the actuated revolute joints are measured ($C = 4$). For this mechanism, the $dosr$ is equal to 1. So, in the "perfect" case, this mechanism with actuation redundancy is "over-measured".

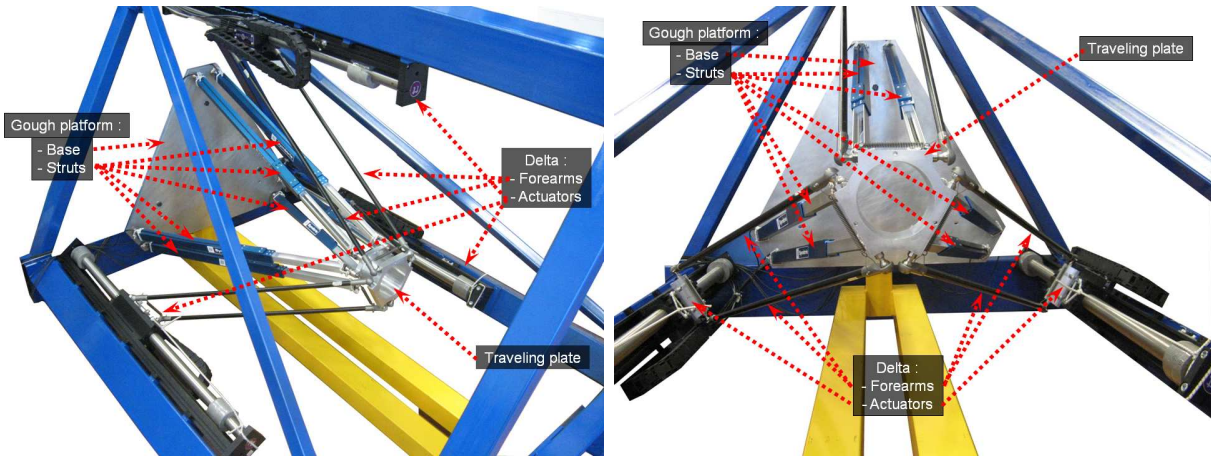
3.3 Conclusion

It will often be necessary to consider that M is equal to 6 (position and orientation of the end-effector in space) since it is difficult to cancel all the errors which cause parasitical movements. But, if the parasitical movements are negligible compared with the required accuracy, then the perfect case can be applied ($M = O$). Of course, the definition of *dosr* given here is just a first indication of what is needed in terms of number of sensors. Designers have to guarantee that the measures are independent and sensitive to the considered displacements in order to provide an efficient control.

4 MoM3 : Parallel Machine-Tool with Independent Measuring System

Fig. 2 has shown that PKM suffer from the same problems than their serial counterparts: links and joints suffering from deformations due to process forces are included into the measurement chain. It turns out that PKM might be good candidates for designing systems relying on SAM. This section introduces a parallel machine which has been designed respecting the considerations exposed above.

MoM3 is composed of a 3-*dof* actuated linear Delta mechanism and a 6-*dof* measuring passive Gough platform (see prototype in Fig. 8). Figure 9 shows how SAM works on MoM3. The forces applied on the end-effector are transmitted to the ground by the actuated chains while the Gough platform measures directly the end-effector pose without transmitting any force due to the process. The measurement device is also protected from the thermal effects



(a) Side view

(b) Face view

Figure 8: MoM3 Prototype

due to the heat produced by the motors. Note that if heat is produced at the end effector level (e.g.: in the case of a machining spindle, there is always heat produced here) thermal protection should be embedded here.

4.1 Actuation mechanism

MoM3 traveling plate is actuated by a linear Delta mechanism which provides the 3 translational *dof* ($D = 3$, $O = 3$) required for most of the machining tasks [21] as well as for moving a probe in case of measurement applications. The forearms form spatial parallelograms which keep (in the ideal case) the traveling plate orientation constant. The linear Delta robot is a very simple mechanism with high dynamical capacities and it has already proved its efficiency for machining [5] [6]. The optimization of this mechanism is presented in [21]. However, considering an "imperfect case", a Delta mechanism cannot guarantee that the traveling plate moves perfectly along 3 translations. Indeed, if the legs do not have the same length, parasitic motions will occur ($M = 6$).

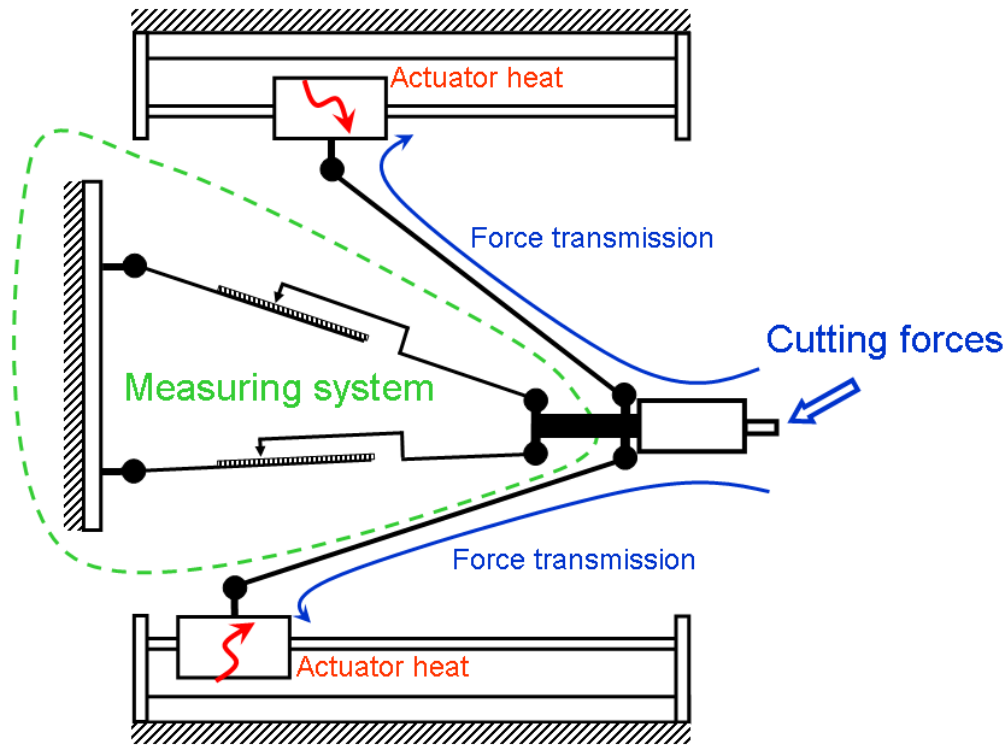


Figure 9: Principle of the SAM on MoM3

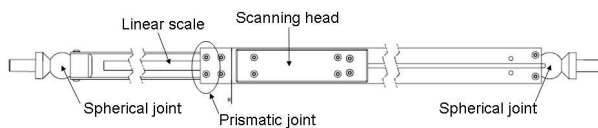
4.2 Measurement mechanism

For MoM3 design, a mechanical measuring system is chosen since, in the current state of our knowledge, it is the best way to have accurate measurements at high frequency [21]. More specifically, the measurement mechanism is a Gough platform which provides the 6 measures ($C = 6$) required to know the complete pose of the end-effector and to have an "iso-measured" MT. Moreover, this architecture has a low impact on the dynamics of the actuation chain and transmits no force. Note that it might be possible to install more than 6 measuring struts and then to obtain $dosr > 0$; this could be used to further increase the accuracy of the system or to provide self calibration capabilities.

4.3 Measurement technology

The measuring struts are composed of telescopic legs with two parts: one mobile part and one fixed part. A linear scale is placed on the mobile part and a scanning head is placed on the fixed part (Fig. 10a). The linear scales have a resolution of $1 \mu\text{m}$ for this first prototype but higher resolution scales are available on the market and could be installed as well. The struts are linked to the base and end-effector by magnetic spherical joints which provide low friction and very low positioning errors (below $1 \mu\text{m}$).

One very important point is that the calibration of the Gough platform is very simple thanks to the use of these measuring struts. Indeed, the struts can be calibrated one by one with a calibration artefact (Fig. 10c). Moreover, the position of the spherical joint centers can be determined accurately with a CMM, since both the Gough platform fixed plate and the traveling plate are small parts which can easily be dismantled and placed on a CMM.



(a) Gough platform strut sketch



(b) Gough platform strut in the calibration artefact. This equipment has been designed following our specifications by Symétrie Co. Nîmes, France.

Figure 10: Gough platform strut and calibration device

5 Optimization of the Gough platform

5.1 Introduction

This section presents the optimization of the Gough platform. The features studied here are the positioning capabilities of the Gough platform. As explained before, the measuring system must have good positioning capabilities: repeatability, resolution and accuracy. These capabilities depend on several factors. Some factors can be controlled during the design process while others cannot. Let's see this for each positioning capability.

First of all, repeatability is extremely dependent on the realization of the joints, the choice of the mechanical elements and the quality of the control. Backlash or friction on the joints can decrease repeatability.

Concerning the machine accuracy, calibration is required to eliminate the positioning errors due to manufacturing and assembly errors. On the designed Gough platform, the calibration is very simple as explained above. Other sources of errors exist as compliance which can be modeled and identified [13]. In our case, the compliance of the Gough platform is neglected since the elements of Gough platform are supposed not to be stressed (except the weight of the struts which is neglected).

Finally, the last capability is the resolution of the mechanism. The first elements which get involved in the mechanism resolution are the active-joint encoders resolution and the controller quality. An other element is the mechanism architecture which is determined during the design phase. Indeed, the transformation between the actuator and end-effector movements depends on the dimensions of the mechanical elements. So, the mechanism theoretical resolution can be improved by an optimization of these dimensions.

The goal of the optimization is to improve the measurement resolution at the tool level. In other words, considering the resolution of the leg encoders, the resolution at the tool level is the minimal displacement of the tool which can be detected by the measuring device. The objective is to have a measuring device which can detect the smallest possible displacement of the tool. The optimization consists in finding the dimensions of the Gough platform which allow to reach this objective. As far as we know, the term “resolution” is correctly defined only for mono-dimensional problems and has, so far, no universally accepted definition for multi-*dof* cases. We try in the following section to propose a “worst case view” of this issue which will give an upper bound of the smallest possible tool displacement.

5.2 Modeling of the Gough platform

Fig. 11 shows the parameters of the Gough platform. Points A_i (B_i , respectively) which represent the centers of the spherical joints on the base (on the traveling plate) are placed on a circle of radius r_b (r_{tp}). Then, three lines passing by the base center O and the traveling plate center E_h and separated by an angle α_0 are defined. Points A_i (B_i) are then located symmetrically to these lines, two by two, with an angle of α_b (α_{tp}).

The measured-joint variables are defined by the Gough platform strut lengths noted l_i ($i \in [1, 6]$). The pose \mathbf{x}_h of the platform is defined by the coordinates x_h, y_h, z_h of the traveling plate center E_h in the base frame \mathcal{R}_b together with 3 angles (yaw, pitch, and roll) ψ_h, θ_h, ϕ_h that allow to calculate the rotation between the base frame \mathcal{R}_b and the traveling plate frame \mathcal{R}_{tp} .

For the optimization of the Gough platform, the positioning errors $\Delta \mathbf{x}_h$ and the length

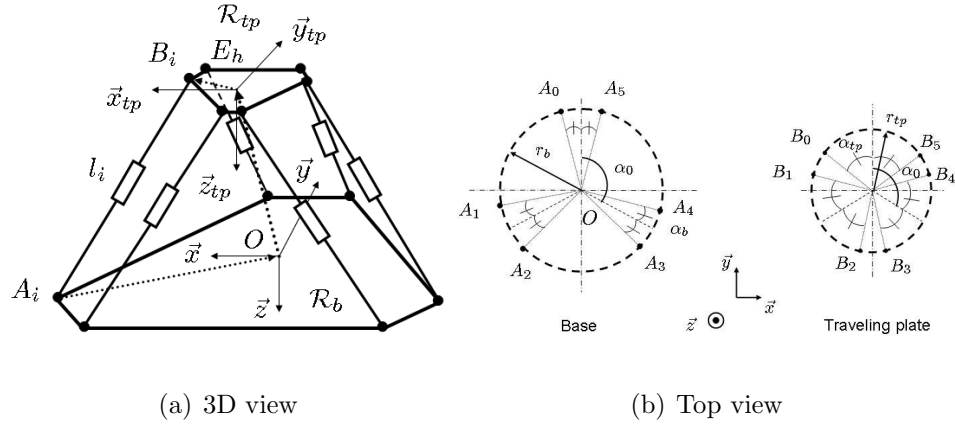


Figure 11: Geometrical parameters of the Gough platform

measurement errors $\Delta \mathbf{l}$ are supposed to be small enough to write an approximation of the error model such as:

$$\Delta \mathbf{x}_h \approx \mathbf{J}_h(\mathbf{P}, \mathbf{x}_h) \Delta \mathbf{l}, \quad (1)$$

where $\mathbf{P} = [r_b, r_{tp}, \alpha_b, \alpha_{tp}]^T$ is the vector of the geometrical parameters and $\mathbf{J}_h(\mathbf{P}, \mathbf{x}_h)$ is the Jacobian matrix of the Gough platform. Only the inverse of the Jacobian matrix has an analytical form which can be calculated as follows:

$$\mathbf{J}_h^{-1} = \begin{bmatrix} \mathbf{u}_1 & -\mathbf{u}_1 \times \mathbf{B}_1 \mathbf{E}_h \\ \vdots & \vdots \\ \mathbf{u}_6 & -\mathbf{u}_6 \times \mathbf{B}_6 \mathbf{E}_h \end{bmatrix}, \quad (2)$$

with

$$\mathbf{u}_i = \frac{\mathbf{A}_i \mathbf{B}_i}{l_i}. \quad (3)$$

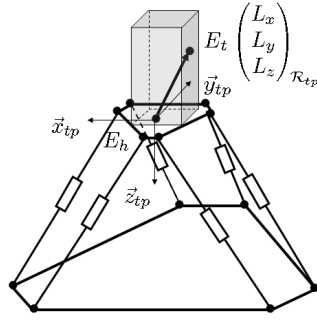


Figure 12: Tool point E_t and its bounding box

5.3 Modeling of the Tool Point

The optimization is performed to obtain the best resolution for the measuring system evaluated at the tool level. But the shape and the size of the tool is unknown since it can change depending on the machining task. The lever arm between the hexapod traveling-plate center E_h and the tool point E_t is variable and is defined by the vector in the base frame \mathcal{R}_{tp} :

$$\mathbf{E}_h \mathbf{E}_t = \begin{bmatrix} L_x \\ L_y \\ L_z \end{bmatrix}_{\mathcal{R}_{tp}} . \quad (4)$$

In the case of this machine, as Delta mechanism imposes the orientation, the vector $\mathbf{E}_h \mathbf{E}_t$ can be considered the same in the base frame and in the traveling plate frame of the Gough platform. The coordinates L_x, L_y, L_z are bounded and the bounding box is presented in Fig. 12.

5.4 Machine Workspace

The MT is designed to machine only small or medium-sized parts. The considered workspace \mathcal{W} is a cube whose sides are 300 millimeters long (Fig. 13). The optimization of the Delta

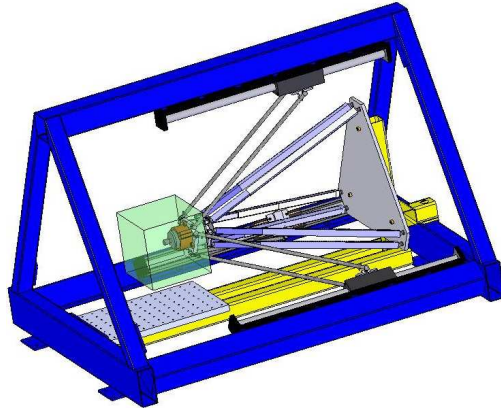


Figure 13: MT workspace \mathcal{W} ($300 \times 300 \times 300 \text{ mm}^3$)

robot and the Gough platform is performed for this workspace.

5.5 Optimization criterion

Two phases are distinguished concerning the Gough platform optimization. First of all, the optimization problem is analyzed considering the tool point as known. Then, the tool bounding box will be considered.

5.5.1 Leg Encoder Errors

Any small displacement of the Gough platform traveling plate, in position $\Delta \mathbf{p}_h$ and orientation $\Delta \mathbf{r}_h$, results in a small displacement of the considered tool point can be approximated by $\Delta \mathbf{p}_t$; this displacement is evaluated at first order as follows:

$$\Delta \mathbf{p}_t = \Delta \mathbf{p}_h + \Delta \mathbf{r}_h \times \mathbf{E}_h \mathbf{E}_t, \quad (5)$$

with

$$\Delta \mathbf{x}_h = \begin{bmatrix} \Delta \mathbf{p}_h \\ \Delta \mathbf{r}_h \end{bmatrix}. \quad (6)$$

From (1), the relation mapping the length measurement errors $\Delta \mathbf{l}$ to the corresponding tool positioning errors $\Delta \mathbf{p}_t$ can be written:

$$\Delta \mathbf{p}_t = \mathbf{J}_{h_P}(\mathcal{P}, \mathbf{x}_h) \Delta \mathbf{l} + \mathbf{J}_{h_R}(\mathcal{P}, \mathbf{x}_h) \Delta \mathbf{l} \times \mathbf{E}_h \mathbf{E}_t, \quad (7)$$

with

$$\mathbf{J}_h(\mathcal{P}, \mathbf{x}_h) = \begin{bmatrix} \mathbf{J}_{h_P}(\mathcal{P}, \mathbf{x}_h) \\ \mathbf{J}_{h_R}(\mathcal{P}, \mathbf{x}_h) \end{bmatrix}. \quad (8)$$

To simplify (7), the second term of its right member is rearranged as follows:

$$\begin{aligned} \mathbf{J}_{h_R} \Delta \mathbf{l} \times \mathbf{E}_h \mathbf{E}_t &= -\mathbf{E}_h \mathbf{E}_t \times \mathbf{J}_{h_R} \Delta \mathbf{l} \\ &= -\widehat{\mathbf{E}_h \mathbf{E}_t} \mathbf{J}_{h_R} \Delta \mathbf{l}, \end{aligned} \quad (9)$$

where $\widehat{\mathbf{E}_h \mathbf{E}_t}$ represents the cross-product matrix.

A small change in the length of the six hexapod struts is mapped into a displacement for the considered tool point by the following relation:

$$\Delta \mathbf{p}_t = \mathbf{J}_t \Delta \mathbf{l}, \quad (10)$$

where

$$\mathbf{J}_t = \mathbf{J}_{h_P} - \widehat{\mathbf{E}_h \mathbf{E}_t} \mathbf{J}_{h_R}, \quad (11)$$

is a 3×6 matrix.

Looking for the 'worst case' requires to find the largest value of $\|\Delta \mathbf{p}_t\|$ (Euclidean norm of the vector $\Delta \mathbf{p}_t$) when each measuring leg encoder suffers from an uncertainty of ε equal to their resolution:

$$-\varepsilon < \Delta l_i < \varepsilon. \quad (12)$$

Due to the linearity of the system (10), for a given point of the workspace and for a given tool point, the maximal value of $\|\Delta\mathbf{p}_t(\mathcal{P}, \mathbf{X}_h)\|$ corresponds to the 2^6 possible combinations corresponding to vectors $\Delta\mathbf{l}$ whose components can be equal to $+\epsilon$ or $-\epsilon$.

5.5.2 Unknown Tool Size

Now, for a given $\Delta\mathbf{l}$ belonging to the 2^6 combinations, the fact that the tool point is considered inside a bounding box has to be taken into account.

Equation (10) can be developed as follows:

$$\Delta\mathbf{p}_t = \begin{bmatrix} \sum_{i=1}^6 J_{1i}\Delta l_i + \sum_{i=1}^6 J_{5i}\Delta l_i L_z - \sum_{i=1}^6 J_{6i}\Delta l_i L_y \\ \sum_{i=1}^6 J_{2i}\Delta l_i + \sum_{i=1}^6 J_{6i}\Delta l_i L_x - \sum_{i=1}^6 J_{4i}\Delta l_i L_z \\ \sum_{i=1}^6 J_{3i}\Delta l_i + \sum_{i=1}^6 J_{4i}\Delta l_i L_y - \sum_{i=1}^6 J_{5i}\Delta l_i L_x \end{bmatrix}, \quad (13)$$

where J_{ji} is the element at j -th row and i -th column of \mathbf{J}_h .

The norm of $\Delta\mathbf{p}_t$ is given by:

$$\begin{aligned} \|\Delta\mathbf{p}_t\| = & \left((S_1 + S_5 L_z - S_6 L_y)^2 \right. \\ & \left. + (S_2 + S_6 L_x - S_4 L_z)^2 + (S_3 + S_4 L_y - S_5 L_x)^2 \right)^{\frac{1}{2}}, \end{aligned} \quad (14)$$

with

$$S_j = \sum_{i=1}^6 J_{ji}\Delta l_i. \quad (15)$$

The squared norm is then studied as a function of L_x, L_y and L_z :

$$f(L_x, L_y, L_z) = \|\Delta\mathbf{p}_t\|^2. \quad (16)$$

Finding the maxima of function $\|\Delta\mathbf{p}_t\|$ is equivalent to finding the maxima of function $\|\Delta\mathbf{p}_t\|^2$.

Briot [22] presents the mathematical background necessary to study this function. He classifies four types of maximum (first, second, third and fourth kind) which are respectively in the whole bounding box, or on the faces, or on the edges or on the corners of the bounding box. Finally, the following functions must be studied:

$$f_1 : (L_x, L_y, L_z) \rightarrow f(L_x, L_y, L_z), f_2 : (L_y, L_z) \rightarrow f(L_{x_{min}}, L_y, L_z),$$

$$f_3 : (L_y, L_z) \rightarrow f(L_{x_{max}}, L_y, L_z), f_4 : (L_x, L_z) \rightarrow f(L_x, L_{y_{min}}, L_z),$$

$$f_5 : (L_x, L_z) \rightarrow f(L_x, L_{y_{max}}, L_z), f_6 : (L_x, L_y) \rightarrow f(L_x, L_y, L_{z_{min}}),$$

$$f_7 : (L_x, L_y) \rightarrow f(L_x, L_y, L_{z_{max}}), f_8 : (L_z) \rightarrow f(L_{x_{min}}, L_{y_{min}}, L_z),$$

$$f_9 : (L_z) \rightarrow f(L_{x_{min}}, L_{y_{max}}, L_z), f_{10} : (L_z) \rightarrow f(L_{x_{max}}, L_{y_{min}}, L_z),$$

$$f_{11} : (L_z) \rightarrow f(L_{x_{max}}, L_{y_{max}}, L_z), f_{12} : (L_y) \rightarrow f(L_{x_{min}}, L_y, L_{z_{min}}),$$

$$f_{13} : (L_y) \rightarrow f(L_{x_{min}}, L_y, L_{z_{max}}), f_{14} : (L_y) \rightarrow f(L_{x_{max}}, L_y, L_{z_{min}}),$$

$$f_{15} : (L_y) \rightarrow f(L_{x_{max}}, L_y, L_{z_{max}}), f_{16} : (L_x) \rightarrow f(L_x, L_{y_{min}}, L_{z_{min}}),$$

$$f_{17} : (L_x) \rightarrow f(L_x, L_{y_{max}}, L_{z_{max}}), f_{18} : (L_x) \rightarrow f(L_x, L_{y_{min}}, L_{z_{min}}),$$

$$f_{19} : (L_x) \rightarrow f(L_x, L_{y_{max}}, L_{z_{max}}),$$

where $L_{x_{min}}, L_{x_{max}}, L_{y_{min}}, L_{y_{max}}, L_{z_{min}}, L_{z_{max}}$ designate the minimal and the maximal values of L_x, L_y, L_z .

The first function f_1 reaches a maximum when its gradient is null and when its hessian matrix is negative definite. The system of equations which described that the gradient is

null is:

$$\begin{cases} S_6(S_2 + S_6L_x - S_4L_z) - S_5(S_3 + S_4L_y - S_5L_x) = 0 \\ -S_6(S_1 + S_5L_z - S_6L_y) + S_4(S_3 + S_4L_y - S_5L_x) = 0 \\ S_5(S_1 + S_5L_z - S_6L_y) - S_4(S_2 + S_6L_x - S_4L_z) = 0 \end{cases} \quad (17)$$

The three equations of this system are not independent. This system represents the equation of a line. Now, it is necessary to study the hessian matrix to qualify the critical points of the function which belong to this line:

$$\mathbf{H}(f_1) = \begin{bmatrix} 2S_5^2 + 2S_6^2 & -2S_5S_4 & -2S_6S_4 \\ -2S_5S_4 & 2S_4^2 + 2S_6^2 & -2S_6S_5 \\ -2S_6S_4 & -2S_6S_5 & 2S_4^2 + 2S_5^2 \end{bmatrix}. \quad (18)$$

This matrix is constant whatever L_x , L_y and L_z . The determinant of this matrix is null and its eigenvalues are $\sigma_1 = 0$ and $\sigma_2 = \sigma_3 = 2S_6^4 + 2S_5^2 + 2S_4^2$. The matrix $\mathbf{H}(f_1)$ is positive semi-definite and the function f has no maximum of the first kind.

Then, the functions f_2, \dots, f_{19} are treated as the first one, that is, analyzing their gradients and hessian matrix. It is determined that there is neither maximum of the second kind nor maximum of the third kind.

Finally, only a maximum of the fourth kind exists and is on one of the eight corners of the tool bounding box.

5.5.3 Global Optimization Criterion

Let $\Omega_{L_x}, \Omega_{L_y}, \Omega_{L_z}, \Omega_{l_0}, \Omega_{l_1}, \Omega_{l_2}, \Omega_{l_3}, \Omega_{l_4}, \Omega_{l_5}$ be the spaces defined by:

$$\begin{aligned}
\Omega_{L_x} &= \{L_{x_{min}}, L_{x_{max}}\}, \quad \Omega_{L_y} = \{L_{y_{min}}, L_{y_{max}}\}, \\
\Omega_{L_z} &= \{L_{z_{min}}, L_{z_{max}}\}, \quad \Omega_{l_0} = \{l_0 - \varepsilon, l_0 + \varepsilon\}, \\
\Omega_{l_1} &= \{l_1 - \varepsilon, l_1 + \varepsilon\}, \quad \Omega_{l_2} = \{l_2 - \varepsilon, l_2 + \varepsilon\}, \\
\Omega_{l_3} &= \{l_3 - \varepsilon, l_3 + \varepsilon\}, \quad \Omega_{l_4} = \{l_4 - \varepsilon, l_4 + \varepsilon\}, \\
\Omega_{l_5} &= \{l_5 - \varepsilon, l_5 + \varepsilon\}.
\end{aligned} \tag{19}$$

Let $\Lambda = \Omega_{L_x} \times \Omega_{L_y} \times \Omega_{L_z} \times \Omega_{l_0} \times \Omega_{l_1} \times \Omega_{l_2} \times \Omega_{l_3} \times \Omega_{l_4} \times \Omega_{l_5}$ be the cartesian product of the spaces defined above.

Finally, the optimization criterion is given by:

$$\mathcal{C}_{opt} = \max_{(x_h, y_h, z_h) \in \mathcal{W}} \mathcal{C}_{int}, \tag{20}$$

$$\mathcal{C}_{int} = \max_{\lambda \in \Lambda} \|\Delta \mathbf{p}_t(\mathcal{P}, \mathbf{x}_h, \lambda)\|. \tag{21}$$

Then, the optimization consists in finding the vector of parameters \mathcal{P}^* which minimize the criterion \mathcal{C}_{opt} .

5.6 Gough platform parameters

The Gough platform optimization has to take into account the Delta geometry to avoid collisions. The distance between the center of both mechanisms is chosen such as it is the smallest possible to minimize the size and the weight of the traveling plate. This distance is equal to 0.1 m. The Gough platform leg lengths can vary between two bounds chosen by the designers ($l_i \in [634 \text{ mm}, 1080 \text{ mm}]$) [23].

The final values of Gough platform are presented in Table 1. Only the final value of r_{tp} is equal to the maximal bound of the interval defined for the optimization. This maximal

Table 1: Gough platform parameters

r_b	r_{tp}	α_b	α_{tp}
375 mm	75 mm	6 °	40 °

bounds were defined such as there is no possibility to have collision between the hexapod legs and the delta ones. The results confirm our preliminary study. The optimization criterion is better when r_{tp} is bigger.

The theoretical resolution of the measuring system is about 6 μm in position and about 30 μrad in orientation. Concerning the theoretical resolution at the tool level, it depends on the distance between the tool point E_t and the Gough platform traveling plate center E_h . In the worst case, with $L_x \in [-0.01\text{m}, 0.01\text{m}]$, $L_y \in [-0.01\text{m}, 0.01\text{m}]$ and $L_z \in [0\text{m}, 0.2\text{m}]$, the resolution evaluated at the tool level reaches 12 μm for a resolution of the legs encoders of 1 μm . This final resolution is little bit high for very accurate machining but it is easy to decrease the resolution of the measuring system by selecting encoders with better resolution.

6 MoM3 Control

6.1 Introduction

The control of the prototype is insured via a lab-made I/O board plugged into the PCI bus of a PC (Windows 2000) and RTX (Real Time eXtension) which is used as a real time software to ensure the control task periodicity. The control task runs at a 2kHz frequency.

Two control schemes are presented in this section. Both of them use a PI control and a velocity feedforward. The first control scheme, called operational measured space control,

uses the Gough platform as a “black box” in the feedback loop which gives the TCP pose (Tool Center Point, equivalent to the end-effector controlled point). In the second control scheme, called sensor space control, the strut length measurements are directly used for the feedback. These control schemes are respectively equivalent to the position-based visual servoing (PBVS) and the image-based visual servoing (IBVS) [24].

6.2 Modeling and notations

Several models, derived in [21], are used in the control schemes: the direct kinematic modeling of the Gough platform (DKM_{GP}), the inverse kinematic modeling of the Gough platform (IKM_{GP}), the Delta robot jacobian matrix \mathbf{J}_d and the Gough platform jacobian matrix \mathbf{J}_h . On the control schemes, the matrix \mathbf{J}_t represents the matrix which maps a small change in the length of Gough platform struts to a small displacement of the TCP. Matrices ${}^t\mathbf{T}_h$ (respectively ${}^h\mathbf{T}_t$) represent the rigid transformation between the TCP frame and the Gough platform frame (respectively between the Gough platform frame and the TCP frame).

Some notations are used in the control schemes:

- $\mathbf{p}_{t_{des}}$ and $\mathbf{p}_{t_{mes}}$ are the desired and measured position of the TCP,
- \mathbf{x}_h is the pose of the Gough platform traveling plate,
- \mathbf{l} is the vector of the Gough platform strut lengths. \mathbf{l}_{des} represents the vector of the desired lengths in the case of the sensor space control,
- $\dot{\mathbf{q}}_d$ is the Delta joint velocity.

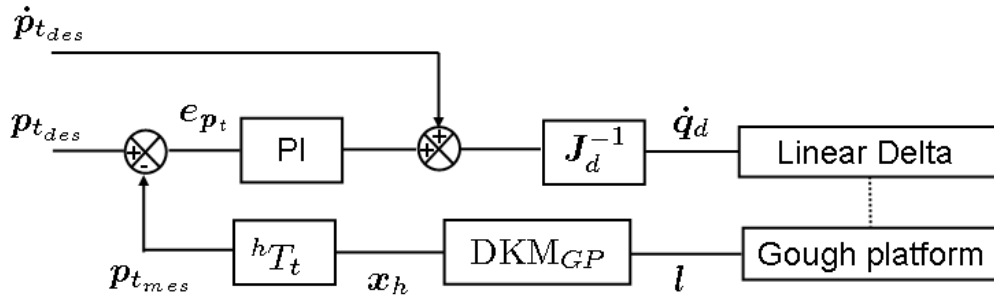


Figure 14: Control scheme of MoM3 in operational measured space

6.3 Operational measured space control

In the operational measured space control, the DKM_{GP} appears explicitly (Fig. 14). This model is calculated with a Newton-Raphson algorithm even though Daney showed that this method may yield numerical instabilities [25]. However, the orientation of the traveling plate is very small and there is no singularities in the workspace, so, in this case, the use of the Newton-Raphson algorithm is acceptable. However, it seems more rigorous to make a control scheme without the Gough platform DKM. That's why a sensor space control is proposed.

6.4 Sensor space control

As explained before, sensor space control is equivalent to IBVS when the measuring system is a camera. In this control scheme (Figure 15), the feedback is made in the sensor space, here on the Gough platform strut lengths. Then, the matrix \mathbf{J}_t transforms the length errors \mathbf{e}_l in TCP pose errors $\mathbf{e}_{\mathbf{p}_t}$ which are the inputs of the PI control.

The difficulty of this control scheme is at level of the trajectory generation. Indeed, as the Delta robot is only a *3-dof* mechanism, the parasitical orientation of the traveling plate cannot be compensated. So, the desired strut lengths \mathbf{l}_{des} cannot be reached since

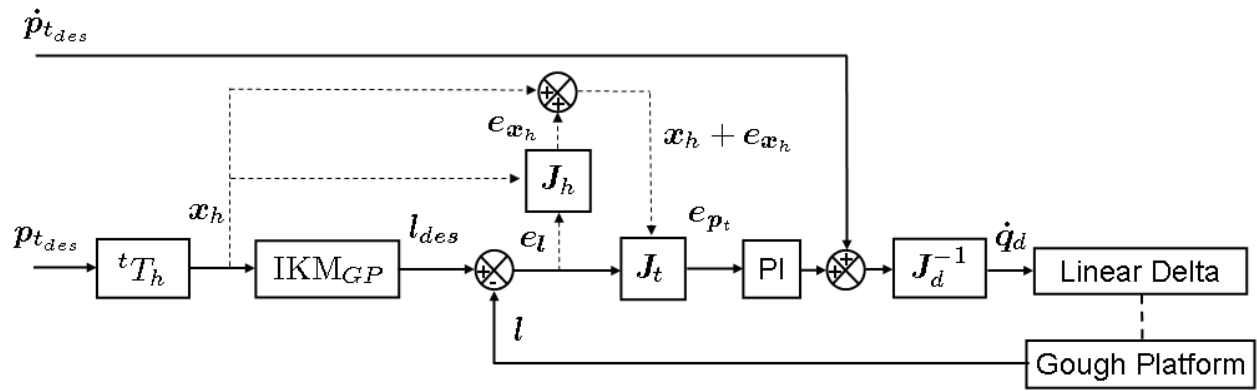


Figure 15: Control scheme of MoM3 in sensor space

they correspond to an unreachable null orientation of the traveling plate. That's implies e_{l_t} is never null. To reach e_{p_t} equal to 0 nevertheless, the matrix J_t must be calculated for the real pose of the Gough platform. If the matrix J_t is calculated at the desired pose of the Gough platform an error of about some microns remains. That's why the pose error of the Gough platform e_{x_h} used for the calculation of matrix J_t is estimated. This estimation allows to cancel the static pose error.

Operational measured space control and sensor space control give similar results but in order to avoid the possible instabilities of the DKM_{GP}, the second one is used for the experimentations.

7 Experimental results

7.1 Validation of the measuring system

Before testing the sensor space control, the measuring system must be validated. To do that, an external measuring system, a laser distancemeter is used. The goal is to show that, when a

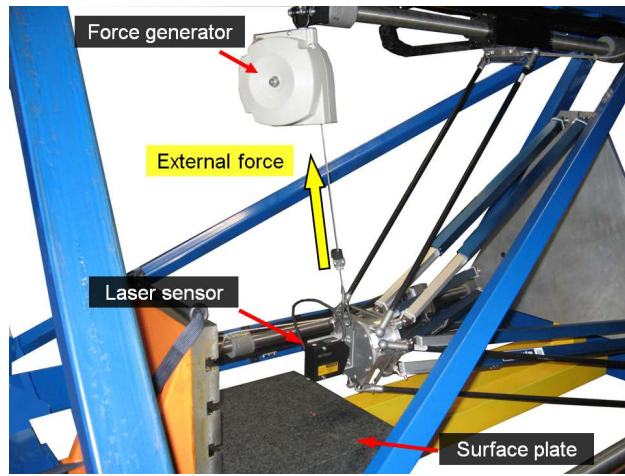


Figure 16: Experimental set-up for the measuring system validation with end-effector load. An external force is applied on the actuation chain, the measuring system can measure the displacement of the end-effector due to the structure deformation. So, the measurement made by the Gough platform and by the laser distancemeter are compared to see if the Gough platform is efficient to measure these small displacements.

7.1.1 End-effector perturbation

Figure 16 shows the experimental set-up with an external force applied on the end-effector.

The experimental device is composed of:

- a surface plate with an absolute flatness lower than $1.6 \mu\text{m}$,
- a Keyence laser distancemeter with a resolution of $0.2 \mu\text{m}$,
- a 80 N to 110 N force generator.

The validation consists in applying a load at the end-effector level and to verify that the Gough platform detects the Delta mechanism deformation. To do that, the Delta robot is

Table 2: Displacement along y axis between a controlled point P_i ($i = 1, 2, 3$), reached by the robot without load, and the same point with a 110 N force applied on the end-effector.

Displacement in μm seen by	P_1	P_2	P_3
the Delta robot	0.3	1	0.6
the Gough platform	73.7	73.1	70.9
the laser distancemeter	80.4	74.4	76.1

controlled from a classical Cartesian control and moved to a point above the surface plate. Measurements from the distancemeter and from the Gough platform (using the DKM_{GP}) are taken and the end-effector pose is calculated from the Delta robot DKM. Then, a 110 N force is applied on the traveling plate and the displacement detected by the three systems (the distancemeter, the Gough platform, the Delta robot) are recorded. Table 2 shows the results for three measurement points.

First of all, the results show the Delta robot control cannot “see” the deformations implied by the load. The Gough platform detects displacements of about 70 μm when a force is applied on the end-effector. These measurements are confirmed by the distancemeter. The measurements made by the Gough platform and the distancemeter are very close and the little differences can be explained by the resolution of the Gough platform evaluated at about 6 microns.

7.1.2 Delta mechanism frame perturbation

A second validation was made with a load applied on the frame (Figure 17). A 850 N force is applied on the Delta frame by a person seated on the top of the frame. Then, the procedure

is the same than above. Table 3 shows the results for three measurement points.

These results confirm the first ones obtained with the load applied on the end-effector. The Gough platform is validated on y axis and considering the symmetry of Gough platform, these results can be extrapolated to z axis and x axis.

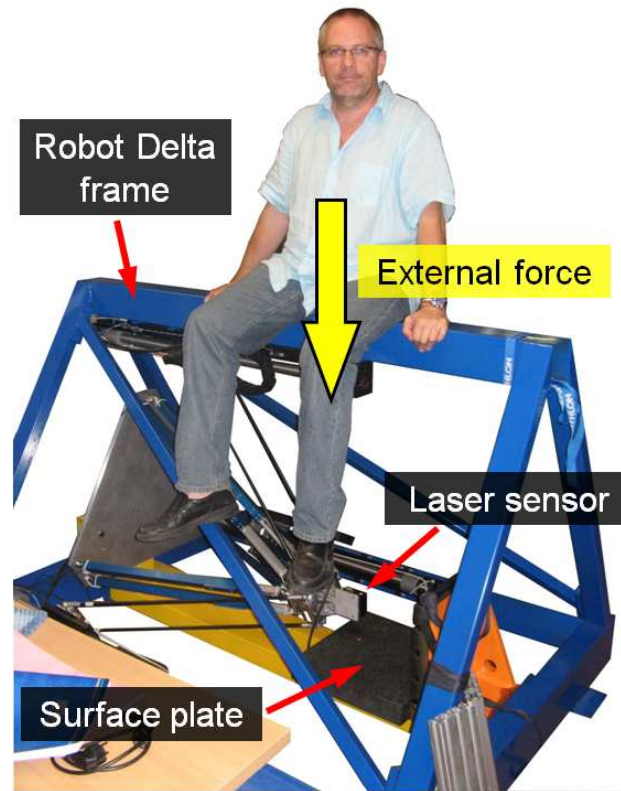


Figure 17: Experimental set-up for the measuring system validation with frame load

Table 3: Displacement along y axis between a controlled point P_i ($i = 1, 2, 3$), reached by the robot without load, and the same point with a 850 N force applied on the Delta frame

Displacement in μm seen by	P_1	P_2	P_3
the Delta robot	1	0.35	1
the Gough platform	70.1	69.2	64.8
the laser distancemeter	65.7	54.8	54.9

These results show equally that the Gough platform can detect the Delta frame deformation and thus they can be compensated with control.

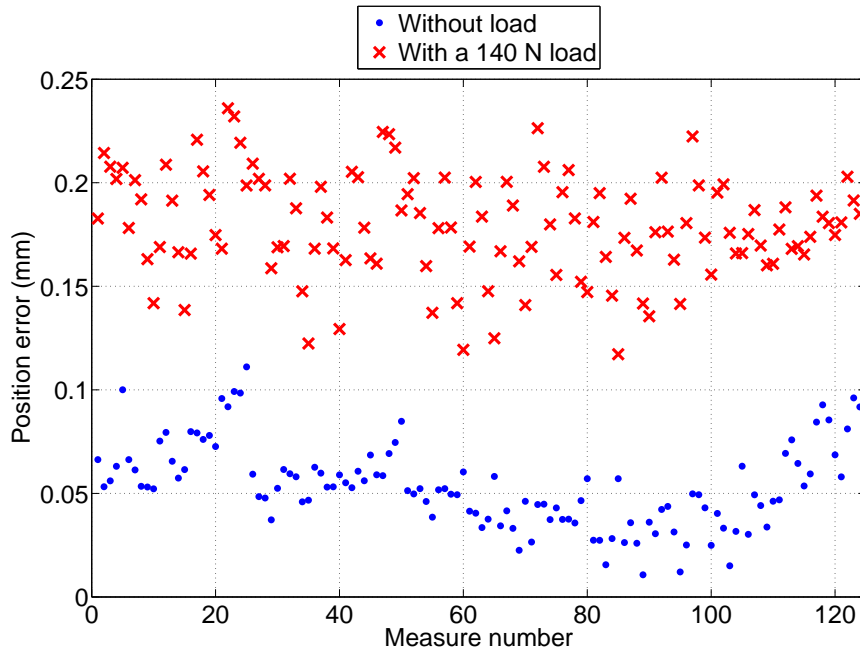
7.2 Sensor space control with external force on the end-effector

In this section, the sensor space control is tested. Two different control are compared: the classical Cartesian Delta mechanism control and the sensor space control. To understand the interest of SAM, a load is applied on the end-effector and the results obtained with the two different control strategies are compared (Fig. 18).

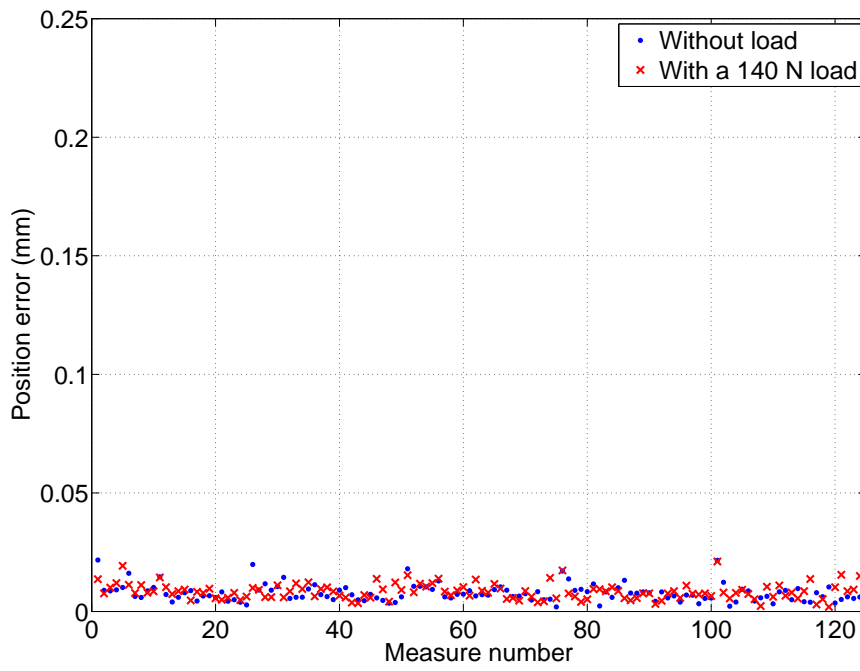
To see the influence of the load, the Delta robot is calibrated (details are available in [23]). Figure 19 shows the results. Sensor space control gives better results (Fig. 19b) than the classical Cartesian control (Fig. 19a) even if the Delta robot is calibrated. Therefore, thanks to SAM, the calibration of the actuation chain is no longer necessary. Moreover, it can be seen from Fig. 19a plots that when the classical Cartesian control is used a 140 N load doubles the end effector position errors. This does not happen when the sensor space control is used (Fig. 19b). So SAM allows to maintain the accuracy of the robot whatever the forces applied on the actuation chain.



Figure 18: 140 N load applied on the MoM3 traveling plate



(a) Classical cartesian control of the calibrated Delta robot



(b) Sensor space control

Figure 19: Comparison of the classical cartesian control and the sensor space control

8 Conclusion

Designing and testing Mom3 has shown the interest of separating Measurement and Actuation when it is applied to parallel mechanisms. In fact, using only well established mechanisms (Delta mechanism for the actuation, Gough-platform for measurement), relying on technologies already in use in precision engineering (magnetic ball joints; linear scale) it has been possible to propose a system offering the following advantages: (i) the measurement chain is independent from the process load, (ii) it can compensate for many deformations encountered in the actuation chain. This has been done thanks to understanding the need of a number of sensors larger than the actuation *dof* (while keeping an “iso-measurement” in our views), optimizing the measurement sub-system so that it can deliver the best resolution (in a “worst case” point of view) and imagining a control strategy which really takes advantage of the system. Based on such advantages, a designer can create machines whose frame or mechanism are not machined or assembled with high precision and can even suffer from permanent deformation. The only requirement would be to guarantee a stiffness suitable for the process. In some cases, a frame, and even a mechanism with most parts made of wood can thus be envisioned, as shown in Fig. 20.

9 Acknowledgement

This work has been partially funded by the European project NEXT, “Next Generation of Production Systems”, Project No. IP 011815.

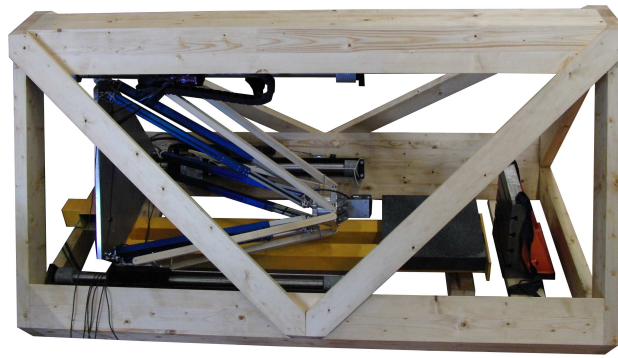


Figure 20: Prototype of MoM3 with a wooden frame and arms

References

- [1] Merlet, J.-P., 2006, *Parallel Robots*, Springer.
- [2] Gough, V. E., 1956-1957, “Contribution to discussion of papers on research in automotive stability, control and tyre performance,” *Proc. Auto Div. Inst. Mech. Eng.*, Institute of mechanical engineering, pp. 392–394.
- [3] Clavel, R., Thurneysen, M., Giovanola, J., and Schnyder, M., 2002, “A new 5 dof parallel kinematics for production applications,” *Proc. of the IEEE International Symposium on Robotics (ISR’02)*, Stockholm, Sweden, pp. 227–232.
- [4] Sheldon, P., 1995, *Six axis machine tool*, US5388935.
- [5] Company, O., Pierrot, F., Launay, F., and Fioroni, C., 2000, “Modelling and preliminary design issues of a 3-axis parallel machine-tool,” *Proc. of the International Conference on Parallel Kinematic Machines PKM’2000*, Ann Arbor, USA, pp. 14–23.
- [6] Krause, E. and Co, 2000, *Machining system with movable tool head*, US6161992.

- [7] Mooring, B. W., Roth, Z. S., and Driels, M. R., 1991, *Fundamentals of Manipulator Calibration*, John Wiley & Sons, Inc., New-York.
- [8] Andreff, N., Renaud, P., Martinet, P., and Pierrot, F., 2004, “Vision-based kinematic calibration of a H4 parallel mechanism: Practical accuracies,” *Industrial Robot International Journal*, **31**(3), pp. 273–283.
- [9] Tlustý, J., Ziegert, J., and Ridgeway, S., 2000, “A comparison of stiffness characteristics of serial and parallel machine tools,” *Journal of Manufacturing Systems*, **2**(2), pp. 67–76.
- [10] Marquet, F., 2002, *Contribution à l'étude de l'apport de la redondance en robotique parallèle*, Ph.D. thesis, Université Montpellier II, Montpellier, France.
- [11] Gosselin, C. M. and Zang, D., 2002, “Stiffness analysis of parallel mechanisms using a lumped model,” *International Journal of Robotics and Automation*, **17**(1), pp. 17–27.
- [12] Ecorchard, G. and Maurine, P., 2005, “Self-calibration of delta parallel robots with elastic deformation compensation,” *Proc. of the IEEE International Conference on Intelligent Robots and Systems (IROS'05)*, Edmonton, Alberta, Canada, pp. 1283– 1288.
- [13] Deblaise, D., Hernot, X., and Maurine, P., 2006, “A systematic analytical method for pkm stiffness matrix calculation,” *Proc. of the IEEE International Conference on Robotics and Automation (ICRA'06)*, Orlando, Floride, USA, p. 42134219.
- [14] Shirai, Y. and Inoue, H., 1973, “Guiding a robot by visual feedback in assembling tasks,” *Pattern Recognition*, **5**, pp. 99–106.

- [15] Dallej, T., Andreff, N., Mezouar, Y., and Martinet, P., 2006, “3D pose visual servoing relieves parallel robot control from joint sensing,” *Proc. of the IEEE International Conference on Intelligent Robots and Systems (IROS’06)*, Beijing, China, pp. 4291–4296.
- [16] David, J., 1989, *Machine à Mesurer par Coordonnées*, FR2627582.
- [17] Hale, L., 1999, *Principles and techniques for designing precision machines*, Ph.D. thesis, University of California, Livermore, California, USA.
- [18] Slocum, A., 1992, *Precision Machine Design*, Prentice-Hall, Inc.
- [19] Lahousse, L., David, J., Leleu, S., Vaillau, G.-P., and Ducourtieux, S., 2005, “Application d’une nouvelle conception d’architecture à une machine de mesure de résolution nanométrique,” *Revue française de métrologie*, **4**(4), pp. 35–43.
- [20] Gogu, G., 2005, “Mobility and spatiality of parallel robots revisited via theory of linear transformations,” *European Journal of Mechanics - A/Solids*, **24**(4), pp. 690–711.
- [21] Corbel, D., Company, O., and Pierrot, F., 2008, “Optimal design of a 6-dof parallel measurement mechanism integrated in a 3-dof parallel machine-tool,” *Proc. of the IEEE International Conference on Intelligent Robots and Systems (IROS’08)*, Nice, France, pp. 1970–1976.
- [22] Briot, S. and Bonev, I., 2007, “Accuracy analysis of 3-DOF planar parallel robots,” *Mech. Mach. Theory*, doi:10.1016/j.mechmachtheory.2007.04.002.
- [23] Corbel, D., 2008, *Contribution à l’amélioration de la précision des robots parallèles*, Ph.D. thesis, Université Montpellier II, Montpellier, France.

- [24] Chaumette, F. and Hutchinson, S., 2006, “Visual servo control, part i: Basic approaches,” *IEEE Robotics and Automation Magazine*, **13**(4), pp. 82–90.
- [25] Daney, D., 1999, “Self calibration of the gough platform using leg mobility constraints,” *10th World Congress on the theory of machine and mechanisms*, Oulu, Finland, pp. 104–109.